THE JOURNAL OF PHYSICAL CHEMISTRY C

Article

pubs.acs.org/JPCC

Electrochemical Reaction of Aqueous Iron Sulfate Solutions Studied by Fe L-Edge Soft X-ray Absorption Spectroscopy

Masanari Nagasaka,*[,†,‡] Hayato Yuzawa,[†] Toshio Horigome,[†] Adam P. Hitchcock,[§] and Nobuhiro Kosugi[†,‡]

[†]Institute for Molecular Science, Myodaiji, Okazaki 444-8585, Japan

[‡]The Graduate University for Advanced Studies, Myodaiji, Okazaki 444-8585, Japan

[§]Department of Chemistry and Chemical Biology, McMaster University, Hamilton, ON L8S 4M1, Canada

ABSTRACT: Change in valence of Fe ions in aqueous iron sulfate solutions at different potentials has been studied by Fe L-edge soft X-ray absorption spectroscopy (XAS) in transmission mode. Each XAS spectrum is measured at a constant potential by using a liquid cell with built-in electrodes. A nonlinear oxidation of Fe(II) ions to Fe(III) ions is observed when the potential is increased from 0.0 to 0.9 V. Two processes are found in the oxidation: one is a simple oxidation process and the other is a process involving the sulfate ions. The potential peak in the latter process is changed with different scanning rates because the sulfate ions affect electrode kinetic parameters and diffusion coefficients. The reduction of Fe(III) ions to Fe(II) ions shows a linear profile when the potential is decreased from 0.9 to −0.4 V. The mechanism of these Fe redox processes is discussed by correlating the XAS results with cyclic voltammetry results at different scanning rates.

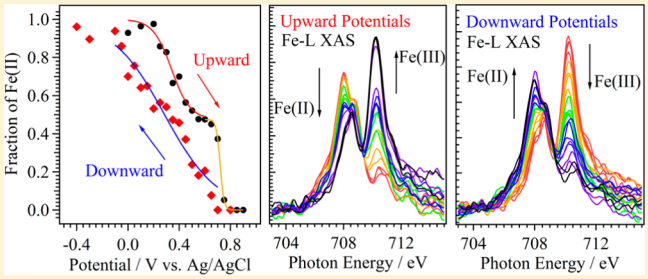

1. INTRODUCTION

To get a better understanding of electrochemistry, it is necessary to know structures of electrolytes including electric double layers at different potentials. The structures of electric double layers were mainly studied by using electrolyte molecules adsorbed on single-crystal electrode surfaces under vacuum. For example, the structural changes of surface adsorbates at different potentials were studied by X-ray photoelectron spectroscopy.[1] The surface distributions of adsorbates were investigated by scanning tunneling microscopy[2] and atomic force microscopy.[3] However, the structures of surface adsorbates under vacuum are different from those under atmospheric conditions. There is no information on electrolytes in bulk phase. It is important to investigate the structures of electrolyte molecules at solid−liquid interfaces of electrodes under realistic conditions.

The structures of solvent water molecules at different potentials were determined from OH stretching mode in Fourier transform infrared spectroscopy.[4,5] The adsorption structures of water molecules were studied by methods focusing on solid−liquid interfaces, such as sum frequency generation,[6] surface-enhanced Raman,[7] and surface-enhanced infrared spectroscopy.[8] The orientation of water molecules at the first layers of Ag(111) electrodes was revealed to be changed at different potentials in 0.1 M NaF by X-ray scattering.[9] The distributions of electrodeposited nanoparticles on electrode surfaces were observed by transmission electron microscopy.[10]

The structures of electrolyte molecules at solid−liquid interfaces of electrodes have been studied extensively by several methods, but there are few studies by direct measurement of the change in valence and structure with element-specific spectroscopy. It is also difficult to investigate the structure of electrolytic solutes in dilute electrolyte solutions.

X-ray absorption spectroscopy (XAS) is a powerful tool to study local electronic structures and is applicable to liquids. The element-specific spectra of solutes can be observed even in dilute solutions. Nakai et al. developed a liquid cell for XAS of electrolyte solutions and revealed dynamic changes of Mn ions in solution by measuring Mn K-edge XAS.[11] Endo et al. studied adsorption structures of Br ions on Ag(100) surfaces at different potentials in aqueous NaBr solutions by measuring Br K-edge XAS.[12] The structures of electrodeposited Ni−B films were investigated by Ni K-edge XAS.[13] Wu et al. used Cu K-edge XAS to investigate the effect of different anions on the structure of underpotential deposition of Cu on Au.[14,15] All of those measurements were performed in the hard X-ray region, in which XAS spectra are easily measured in transmission or fluorescence mode due to the high transmittance of hard X-rays. However, XAS in the hard X-ray region is not applicable to electrolytes including chemically important elements such as C, N, and O. It is necessary to probe these electrolytes during electrochemical reaction.

The soft X-ray region below ∼2 keV has many chemically important absorption edges such as C, N, and O K-edges. Recently, the structure of liquid water has been extensively studied by O K-edge XAS.[16−18] Because the X-ray absorption

Received: May 24, 2013
Revised: July 11, 2013
Published: July 16, 2013

   dx.doi.org/10.1021/jp405112r | J. Phys. Chem. C 2013, 117, 16343−16348

process occurs within several femto seconds, XAS is able to investigate hydrogen-bonding networks in liquid water before reconstruction of the networks. XAS spectra of liquid samples can be measured by different methods from transmission mode:[19,20] fluorescence yield,[17] nonresonant Raman technique,[18] total electron yield of liquid microjet,[16] and inverse partial fluorescence yield of liquid microjet.[21−24] Comparison with the transmission spectra is discussed as regards background subtraction, normalization, and saturation-correction. Note that XAS in bulk liquid phase measured by nonresonant Raman and inverse partial fluorescence yields is nearly the same as XAS in transmission mode. Because soft X-rays at the O K-edge are strongly absorbed by water itself in XAS measured in transmission mode, it is necessary to keep the thickness of the liquid layer below a few micrometers.[25] Therefore, it is difficult to measure XAS of liquid samples in transmission mode. It has not been applied previously to XAS studies of electrochemical reactions of electrolytes.

Recently, we have developed a liquid cell for XAS in transmission mode.[19] The liquid layer is sandwiched between two Si_3N_4 membranes and is kept at atmospheric pressure. The liquid sample is under realistic conditions. The thickness of the liquid layer is controllable between 20 and 2000 nm. We have studied the hydration structure of different cations in aqueous salt solutions by the O K-edge XAS and the local structure of methanol−water binary solutions at different mixing ratios by the C and O K-edge XAS. This liquid cell is also able to measure XAS of solid−liquid interfaces by depositing a solid substrate on the membrane and adjustingt the thickness of the liquid layer as small as possible (<20 nm).

In the present work, we have developed an in situ XAS measurement system to study electrochemical reactions of electrolytes under realistic conditions by using a liquid cell with built-in electrodes. Change in valence of Fe ions in an aqueous iron sulfate solution at different potentials is investigated by Fe L-edge XAS spectra. The redox reaction of Fe ions is one of the most common electrochemical systems because of their importance in a variety of fields. Previously, Fe redox reactions were mainly studied by voltammetric methods,[26−35] but it is difficult to know the change in valence of Fe ions at different potentials in dilute electrolyte solutions. The Fe L-edge (700 eV) is more sensitive than the Fe K-edge to the 3d valence and spin states of Fe ions.[36−43] Here we report direct Fe L-edge XAS measurement of the change in valence of Fe ions induced by variation of the potential at a gold electrode.

2. EXPERIMENTAL METHODS

The experiments were performed on the soft X-ray undulator beamline BL3U at the UVSOR-III facility.[44] Figure 1a shows schematics of the present liquid cell. As previously described,[19] the liquid cell consists of four regions I, II, III, and IV, separated by 100 nm-thick Si_3N_4 membranes (NTT AT Co.). SiC membranes are used for the N K-edge. Region I is connected to the beamline under vacuum. Regions II and IV are at atmospheric pressure of helium buffer gas. The flow rate of the buffer gas is changeable by a mass flow controller, and the pressure is adjusted by a needle valve at the gas outlet. The thin liquid layer (region III) is sandwiched between two Si_3N_4 membranes, each with a window size of 2 mm × 2 mm. The liquid layer is under atmospheric conditions. Two 100 μm thick spacers are set between the window frames of the membranes, and the membranes are compressed by sealing o-rings to keep the thin liquid layer below 2000 nm. Liquid samples can be

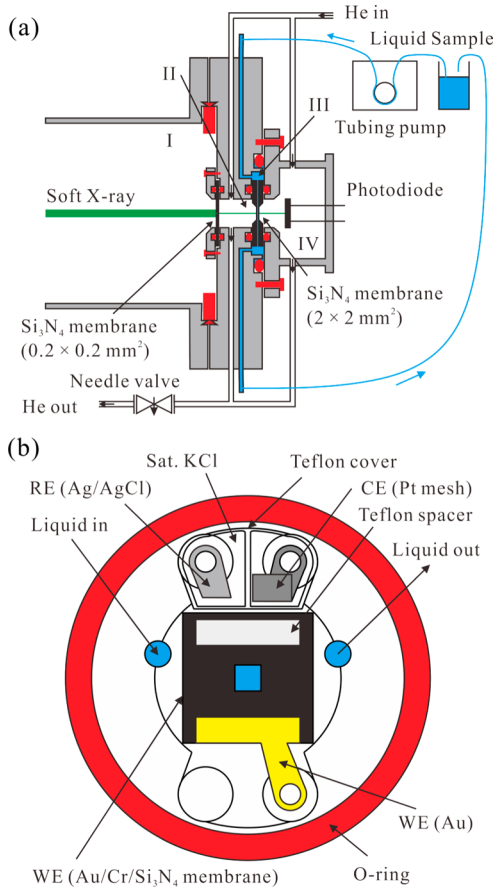

Figure 1. (a) Schematic of the liquid cell for XAS in transmission mode. The details of the liquid cell are described in the text. (b) Schematics of three electrodes included in the liquid layer (region III). The working electrode (WE) is Au-deposited on a Si_3N_4 membrane. The counter electrode (CE) is a Pt mesh. The reference electrode (RE) is Ag/AgCl immersed in a saturated KCl solution.

exchanged in situ with a tubing pumping system. The thickness of the liquid layer is controllable between 20 and 2000 nm by changing the He pressure in regions II and IV.[19] The absorption of soft X-rays in regions II and IV is small due to the high transmittance of helium.[25] The size of the Si_3N_4 membrane window between regions I and II is 0.2 mm × 0.2 mm, which is small enough to endure a large difference in pressure (>1 atm). The soft X-ray beam size on the sample is determined by this orifice. Although the thickness of the liquid layer varies at different positions over the 2 mm × 2 mm membranes, it is possible to measure XAS of the liquid layer at a constant thickness because of the small beam size.[19] Soft X-rays, which pass through region II and the liquid layer (region III), are detected by a photodiode (IRD AXUV100) in region IV. The photon energy resolution at the Fe L-edge was set to 0.7 eV. The XAS spectra are obtained from the measured transmission signal, by the Lambert−Beer formula $\ln(I_0/I)$, in which the current I_0 is measured for pure liquid water and the current I is for the liquid sample. The photon energy is calibrated by the O 1s−π^* peak (530.80 eV)[45] for O_2 gas as mixed in a buffer gas with He gas in regions II and IV.

For the investigation of electrochemical reactions, three electrodes are included in the liquid layer (region III), as shown in Figure 1b. In the present work, the electrolyte is 0.5 M aqueous iron sulfate at pH 2.2. The working electrode is a Au

dx.doi.org/10.1021/jp405112r | J. Phys. Chem. C 2013, 117, 16343−16348

deposit on one of the Si_3N_4 membranes, which consists of Au (10 nm), Cr (5 nm), and Si_3N_4 (100 nm) multilayer films. This membrane is one side of the liquid layer and is connected with the Au tab for electrical conduction. The Teflon spacer is placed on the Si frame, opposite the Au contact. The counter electrode is a Pt mesh, which is immersed in the sample electrolyte solution. The reference electrode is Ag/AgCl immersed in a saturated KCl solution and isolated from the liquid sample by a Teflon cover. The potential is controlled by using a potentiostat (Solartron 1287). We have confirmed from the Fe L-edge XAS of the Au-deposited membrane that the membrane has no deposition of Fe metals or compounds after and also during the Fe redox reaction.

3. RESULTS AND DISCUSSION

3.1. Cyclic Voltammetry. Figure 2 shows cyclic voltammetry (CV) spectra of a 0.5 M aqueous iron sulfate solution measured by using a conventional electrochemical cell. The working, counter, and reference electrodes are Au, Pt, and Ag/AgCl with 3 M NaCl, respectively. The CV spectrum shown in Figure 2a was measured at a scanning rate of 20 mV/s. The oxidation of Fe(II) ions to Fe(III) ions with increasing potential is observed as the peak at 0.70 V. When the potential is decreased, the reduction of Fe(III) ions to Fe(II) ions is observed as the peak at 0.29 V.

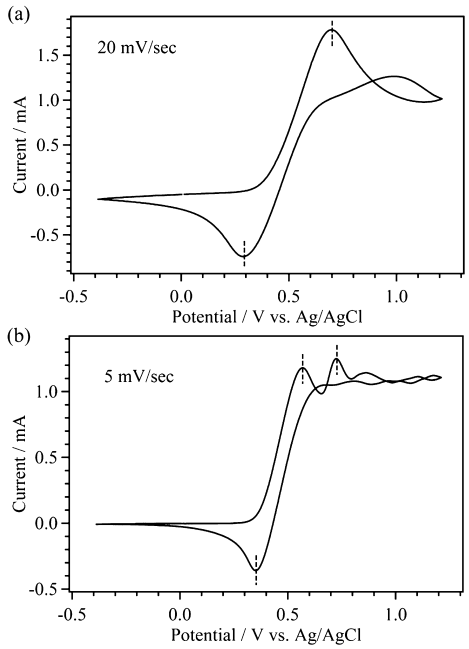

Figure 2. CV spectra of 0.5 M aqueous iron sulfate solutions with scanning rates of (a) 20 and (b) 5 mV/s. The horizontal axis is the potential of the Au electrode versus the Ag/AgCl reference electrode. The peak positions of the CV spectra are listed in Table 1.

Figure 2b shows a CV spectrum measured at a scanning rate of 5 mV/s. The reduction of Fe(III) ions to Fe(II) ions occurs as a single peak at 0.35 V, which is close to that obtained at 20 mV/s. The oxidation of Fe(II) ions to Fe(III) ions shows two peaks, whose positions are 0.57 and 0.72 V. The peak at 0.72 V is close to that obtained at 20 mV/s and is attributed to simple oxidation of Fe(II) to Fe(III). The oxidation process at the low potential involves the sulfate ions, which affect electrode kinetic parameters and diffusion coefficients[34,35] at high concentration of aqueous iron sulfate solutions.[27,28,33] The peak positions are summarized in Table 1.

Table 1. Peak Positions of the Fe Redox Reactions in an Aqueous Iron Sulfate Solution with the Different Scanning Rates Measured by CV and XAS Spectra[a]

potential (V)	P1	P2
Oxidation of Fe(II)		
0.08 mV/s (XAS)	0.72	0.34
5 mV/s (CV)	0.72	0.57
20 mV/s (CV)	0.70	
Reduction of Fe(III)		
0.08 mV/s (XAS)	0.29	
5 mV/s (CV)	0.35	
20 mV/s (CV)	0.29	

[a]Oxidation of Fe(II) ions has two processes. One is the simple oxidation (P1) and the other involves the sulfate ions (P2). The reduction of Fe(III) ions is a single process (P1).

3.2. Fe L-edge XAS. Figure 3 shows Fe L-edge XAS spectra of aqueous iron sulfate solutions at different potentials. Each XAS spectrum is measured at a constant potential. The Fe L-edge XAS spectra were measured by increasing the potential from 0.00 to 0.90 V, as shown in Figure 3a. The XAS measurements continued, while the potential was decreased from 0.90 to −0.40 V, as shown in Figure 3b. The scanning rate of the potential is roughly estimated to be 0.08 mV/s, which is slower than those of the CV measurements. The XAS L_3 spectra have signals from both Fe(II) and Fe(III) ions and show an isosbestic point, indicating that only two species are involved.

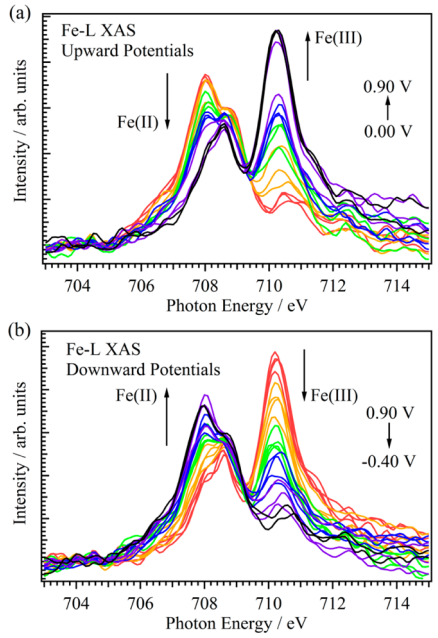

Figure 3. Fe L-edge XAS spectra of Fe ions in a 0.5 M aqueous iron sulfate at different potentials: (a) increasing from 0.00 to 0.90 V and (b) decreasing from 0.90 to −0.40 V.

Figure 4a shows reference Fe L-edge XAS spectra for Fe(II) and Fe(III) ions in aqueous iron sulfate solutions. The XAS spectrum of Fe(II) ions was measured at no applied potential, whereas that of Fe(III) ions was obtained at an applied

dx.doi.org/10.1021/jp405112r | J. Phys. Chem. C 2013, 117, 16343−16348

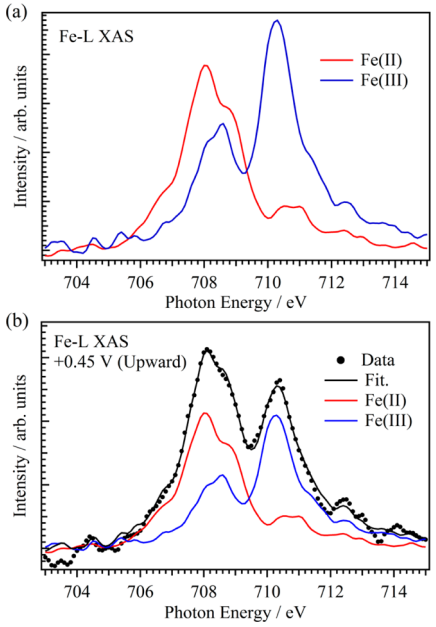

Figure 4. (a) Reference Fe L-edge XAS spectra for Fe(II) and Fe(III) ions in aqueous iron sulfate solutions. (b) Example of the fitting of the Fe L-edge XAS spectrum at the potential of 0.45 V in the upward direction by superposition of the reference spectra.

potential of 0.90 V. As shown in Figure 3a, the amount of Fe(II) ions decreases to form Fe(III) ions nonlinearly when the potential is increased. When the potential is decreased, a linear change of the XAS spectra from Fe(III) ions to Fe(II) ions is observed, as shown in Figure 3b. To obtain the fraction of Fe(II) and Fe(III) ions, we fit the Fe L-edge XAS spectra at different potentials to a superposition of the reference spectra of Fe(II) and Fe(III) ions shown in Figure 4a. Figure 4b shows an example of the least-squares fitting for the Fe L-edge XAS spectrum measured at a potential of 0.45 V in the upward scanning direction. There is good agreement with a simple superposition of the reference spectra.

3.3. Mechanism of Fe Redox Reactions. Figure 5 shows the fraction of Fe(II) ions (Fe(II) + Fe(III) = 1.0) as a function of potential and scanning direction. The uncertainty of the measured fractions is estimated to be within ±0.02. The composition is determined from the curve fitting of the XAS spectra. The amount of Fe(II) ions decreases by oxidation of Fe(II) to Fe(III) with increasing the potential, which consists of two processes, as indicated by the change in slope of the composition curve at 0.7 and 0.4 V. The formation of Fe(II) from Fe(III) with decreasing potential is linear, indicating a single-step reduction of Fe(III) ions. The fraction of Fe(II) ions $C_{Fe(II)}$ as a function of potential is fit to a sigmoid profile as

$$C_{Fe(II)}(E) = C_{min} + \frac{C_{max} - C_{min}}{1 + \exp[\alpha(E - E_0)]} \quad (1)$$

where E_0 is the central potential and the terms C_{min} and C_{max} are minimum and maximum fractions of Fe(II) ions in the single process, respectively. The slope of the sigmoid profile is influenced by term α.

Table 1 shows the central potentials of the Fe redox process obtained by the fits to sigmoid profiles, together with the results of the CV spectra at the different scanning rates. The oxidation of Fe(II) ions to Fe(III) ions has two processes which occur at potentials of 0.34 and 0.72 V. The reduction of Fe(III) ions to Fe(II) ions occurs at a potential of 0.29 V. Because each XAS spectrum is obtained at a constant potential, the scanning rate of the potential is quite slow (0.08 mV/s) in the XAS measurements as compared with the CV results (5 and 20 mV/s). As shown in Table 1, the reduction peak of Fe(III) ions obtained by XAS is close to that obtained by the CV spectra. The reduction of Fe(III) ions is a simple process that reaches an equilibrium even at a scanning rate of 20 mV/s. The profile of the reduction is deviated slightly from the sigmoid profile. It might be influenced by the sulfate ions forming some complexes with Fe(III) ions.[35] Two processes are found in the case of oxidation of Fe(II) ions. One is a simple oxidation process of Fe(II) to Fe(III). This peak position is 0.72 V at 0.08 mV/s and is close to that observed in the CV spectra, suggesting that the simple oxidation process reaches equilibrium. The peak position of the other oxidation process is 0.34 V at 0.08 mV/s. In the CV spectra, the peak position is 0.57 V at 5 mV/s, and it is not observed at 20 mV/s. The reason why the peak position varies with the scanning rate is that this oxidation process does not reach equilibrium. The rate of this process is dominantly influenced by the sulfate ions, which affect electrode kinetic parameters and diffusion coefficients.[27,28,33−35] The present XAS results on the change in valence of Fe ions at different scanning rates are consistent with the CV results.

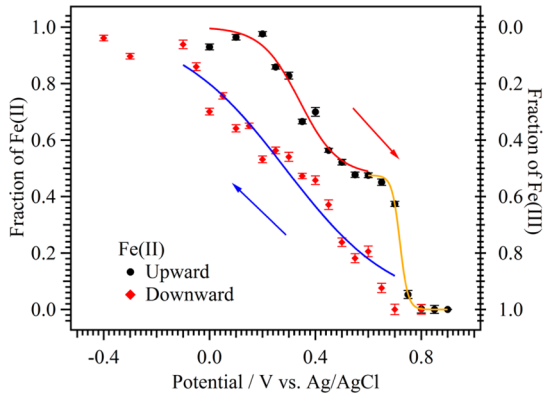

Figure 5. Fraction of Fe(II) ions as a function of potential versus Ag/AgCl with saturated KCl solutions. The arrows indicate the scanning direction of applied potential. Each fraction includes an error bar, which is within ±0.02. The oxidation of Fe(II) with increasing potential has two processes, whereas the reduction of Fe(III) with decreasing potential is a single process. The central potentials of these Fe redox processes are listed in Table 1.

4. CONCLUSIONS

The change in valence of Fe ions in aqueous iron sulfate solutions at different potentials under realistic conditions has been investigated by Fe L-edge XAS in transmission mode. Each X-ray absorption spectrum was measured at a constant potential by using a newly developed liquid cell with built-in electrodes. The Fe redox process is investigated by correlating the XAS results with the CV spectra. The scanning rate of the potential used in the XAS study is estimated to be 0.08 mV/s, which is quite slow compared with that of the CV spectra (5 and 20 mV/s). The reduction of Fe(III) ions to Fe(II) ions with decreasing potential is a single process that reaches equilibrium even at a scanning rate of 20 mV/s. The oxidation of Fe(II) ions to Fe(III) ions with increasing potential consists

dx.doi.org/10.1021/jp405112r | J. Phys. Chem. C 2013, 117, 16343−16348

of two processes. The process at a high potential is simple oxidation of Fe(II) ions that reaches equilibrium even at a scanning rate of 20 mV/s. The oxidation process at a low potential involves the sulfate ions. The peak positions are dependent on the scanning rate because the rate of this process is dominantly influenced by the sulfate ions, which affect electrode kinetic parameters and diffusion coefficients.[27,28,33−35]

In the present study, the change in valence of Fe ions at different potentials leads to a drastic change in the XAS spectra. Therefore, the change in valence of Fe ions can be successfully studied by measurements of the XAS spectrum at a constant potential. However with the present method it is difficult to observe small spectral changes in the XAS spectra at different potentials. For such studies it is necessary to measure changes in soft X-ray absorption at a single photon energy while scanning the applied potential. Even a subtle spectral change in the XAS spectrum can be revealed by measurements of the absorption difference with a potential modulation as a function of photon energy. This will enable us to investigate effects of the environment of a target atom and also to determine kinetic parameters in electrochemical reactions at different potential modulation rates. An apparatus to carry out such detailed measurements has been developed and will be used in future experiments.

AUTHOR INFORMATION

Corresponding Author

*E-mail: nagasaka@ims.ac.jp.

Notes

The authors declare no competing financial interest.

ACKNOWLEDGMENTS

This work is supported by JSPS Grants-in-Aid for Scientific Research (Nos. 23685006 and 23245007). We acknowledge the staff members of the UVSOR-III facility for their kind support. A.H. thanks IMS for its support during a research leave in which this work was performed.

REFERENCES

(1) Wakisaka, M.; Suzuki, H.; Mitsui, S.; Uchida, H.; Watanabe, M. Increased Oxygen Coverage at Pt-Fe Alloy Cathode for the Enhanced Oxygen Reduction Reaction Studied by EC-XPS. *J. Phys. Chem. C* **2008**, *112*, 2750−2755.

(2) Cuesta, A.; Kleinert, M.; Kolb, D. M. The Adsorption of Sulfate and Phosphate on Au(111) and Au(100) Electrodes: An in Situ STM Study. *Phys. Chem. Chem. Phys.* **2000**, *2*, 5684−5690.

(3) Umeda, K.; Fukui, K. Observation of Redox-State-Dependent Reversible Local Structural Change of Ferrocenyl-Terminated Molecular Island by Electrochemical Frequency Modulation AFM. *Langmuir* **2010**, *26*, 9104−9110.

(4) Ashley, K.; Pons, S. Infrared Spectroelectrochemistry. *Chem. Rev.* **1988**, *88*, 673−695.

(5) Nakamura, M.; Kato, H.; Hoshi, N. Infrared Spectroscopy of Water Adsorbed on M(111) (M = Pt, Pd, Rh, Au, Cu) Electrodes in Sulfuric Acid Solution. *J. Phys. Chem. C* **2008**, *112*, 9458−9463.

(6) Nihonyanagi, S.; Ye, S.; Uosaki, K.; Dreesen, L.; Humbert, C.; Thiry, P.; Peremans, A. Potential-Dependent Structure of the Interfacial Water on the Gold Electrode. *Surf. Sci.* **2004**, *573*, 11−16.

(7) Pettinger, B.; Philpott, M. R.; Gordon, J. G., II. Further Observations of the Surface Enhanced Raman Spectrum of Water on Silver and Copper Electrodes. *Surf. Sci.* **1981**, *105*, 469−474.

(8) Ataka, K.; Yotsuyanagi, T.; Osawa, M. Potential-Dependent Reorientation of Water Molecules at an Electrode/Electrolyte Interface Studied by Surface-Enhanced Infrared Absorption Spectroscopy. *J. Phys. Chem.* **1996**, *100*, 10664−10672.

(9) Toney, M. F.; Howard, J. N.; Richer, J.; Borges, G. L.; Gordon, J. G.; Melroy, O. R.; Wiesler, D. G.; Yee, D.; Sorensen, L. B. Voltage-Dependent Ordering of Water Molecules at an Electrode-Electrolyte Interface. *Nature* **1994**, *368*, 444−446.

(10) De Jonge, N.; Ross, F. M. Electron Microscopy of Specimens in Liquid. *Nat. Nanotechnol.* **2011**, *6*, 695−704.

(11) Nakai, I.; Shiraishi, Y.; Nishikawa, F. Development of a New in Situ Cell for the X-ray Absorption Fine Structure Analysis of the Electrochemical Reaction in a Rechargeable Battery and Its Application to the Lithium Battery Material, $Li_{1+y}Mn_{2-y}O_4$. *Spectrochim. Acta, Part B* **1999**, *54*, 143−149.

(12) Endo, O.; Kiguchi, M.; Yokoyama, T.; Ito, M.; Ohta, T. In-Situ X-ray Absorption Studies of Bromine on the Ag(100) Electrode. *J. Electroanal. Chem.* **1999**, *473*, 19−24.

(13) Bediako, D. K.; Lassalle-Kaiser, B.; Surendranath, Y.; Yano, J.; Yachandra, V. K.; Nocera, D. G. Structure-Activity Correlations in a Nickel-Borate Oxygen Evolution Catalyst. *J. Am. Chem. Soc.* **2012**, *134*, 6801−6809.

(14) Wu, S.; Lipkowski, J.; Tyliszczak, T.; Hitchcock, A. P. Effect of Anion Adsorption on Early Stages of Copper Electrocrystallization at Au(111) Surface. *Prog. Surf. Sci.* **1995**, *50*, 227−236.

(15) Wu, S.; Shi, Z.; Lipkowski, J.; Hitchcock, A. P.; Tyliszczak, T. Early Stages of Copper Electrocrystallization: Electrochemical and in Situ X-ray Absorption Fine Structure Studies of Coadsorption of Copper and Chloride at the Au(111) Electrode Surface. *J. Phys. Chem. B* **1997**, *101*, 10310−10322.

(16) Smith, J. D.; Cappa, C. D.; Wilson, K. R.; Messer, B. M.; Cohen, R. C.; Saykally, R. J. Energetics of Hydrogen Bond Network Rearrangements in Liquid Water. *Science* **2004**, *306*, 851−853.

(17) Wernet, P.; Nordlund, D.; Bergmann, U.; Cavalleri, M.; Odelius, M.; Ogasawara, H.; Näslund, L.-Å.; Hirsch, T. K.; Ojamäe, L.; Glatzel, P.; Pettersson, L. G. M.; Nilsson, A. The Structure of the First Coordination Shell in Liquid Water. *Science* **2004**, *304*, 995−999.

(18) Huang, C.; Wikfeldt, K. T.; Tokushima, T.; Nordlund, D.; Harada, Y.; Bergmann, U.; Niebuhr, M.; Weiss, T. M.; Horikawa, Y.; Leetmaa, M.; Ljungberg, M. P.; Takahashi, O.; Lenz, A.; Ojamäe, L.; Lyubartsev, A. P.; Shin, S.; Pettersson, L. G. M.; Nilsson, A. The Inhomogeneous Structure of Water at Ambient Conditions. *Proc. Natl. Acad. Sci. U. S. A.* **2009**, *106*, 15214−15218.

(19) Nagasaka, M.; Hatsui, T.; Horigome, T.; Hamamura, Y.; Kosugi, N. Development of a Liquid Flow Cell to Measure Soft X-ray Absorption in Transmission Mode: A Test for Liquid Water. *J. Electron Spectrosc. Relat. Phenom.* **2010**, *177*, 130−134.

(20) Schreck, S.; Gavrila, G.; Weniger, C.; Wernet, P. A Sample Holder for Soft X-ray Absorption Spectroscopy of Liquids in Transmission Mode. *Rev. Sci. Instrum.* **2011**, *82*, 103101.

(21) Achkar, A. J.; Regier, T. Z.; Wadati, H.; Kim, Y.-J.; Zhang, H.; Hawthorn, D. G. Bulk Sensitive X-ray Absorption Spectroscopy Free of Self-Absorption Effects. *Phys. Rev. B* **2011**, *83*, 081106(R).

(22) Gotz, M. D.; Soldatov, M. A.; Lange, K. M.; Engel, N.; Golnak, R.; Könnecke, R.; Atak, K.; Eberhardt, W.; Aziz, E. F. Probing Coster-Kronig Transitions in Aqueous Fe^{2+} Solution Using Inverse Partial and Partial Fluorescence Yield at the L-Edge. *J. Phys. Chem. Lett.* **2012**, *3*, 1619−1623.

(23) Regier, T. Z.; Achkar, A. J.; Peak, D.; Tse, J. S.; Hawthorn, D. G. Dark Channel Fluorescence Observations Result from Concentration Effects Rather than Solvent-Solute Charge Transfer. *Nat. Chem.* **2012**, *4*, 765−766.

(24) Soldatov, M. A.; Lange, K. M.; Gotz, M. D.; Engel, N.; Golnak, R.; Kothe, A.; Aziz, E. F. On the Origin of Dips in Total Fluorescence Yield X-ray Absorption Spectra: Partial and Inverse Partial Fluorescence Yield at the L-Edge of Cobalt Aqueous Solution. *Chem. Phys. Lett.* **2012**, *546*, 164−167.

(25) Chantler, C. T. Detailed Tabulation of Atomic Form Factors, Photoelectric Absorption and Scattering Cross Section, and Mass Attenuation Coefficients in the Vicinity of Absorption Edges in the Soft X-Ray (Z = 30−36, Z = 60−89, E =0.1 keV−10 keV), Addressing Convergence Issues of Earlier Work. *J. Phys. Chem. Ref. Data* **2000**, *29*, 597−1048.

(26) George, P. The Oxidation of Ferrous Perchlorate by Molecular Oxygen. *J. Chem. Soc.* **1954**, *280*, 4349−4359.
(27) Huffman, R. E.; Davidson, N. Kinetics of the Ferrous Iron-Oxygen Reaction in Sulfuric Acid Solution. *J. Am. Chem. Soc.* **1956**, *78*, 4836−4842.
(28) Beukenkamp, J.; Herrington, K. D. Ion-Exchange Investigation of the Nature of Iron(II) in Sulfuric and Perchloric Acid. *J. Am. Chem. Soc.* **1960**, *82*, 3022−3025.
(29) Wells, C. F.; Salam, M. A. Hydrolysis of Ferrous Ions: a Kinetic Method for the Determination of the Fe(II) Species. *Nature* **1965**, *205*, 690−692.
(30) Bockris, J. O. M.; Mannan, R. J.; Damjanovic, A. Dependence of the Rate of Electrodic Redox Reactions on the Substrate. *J. Chem. Phys.* **1968**, *48*, 1898−1904.
(31) Samec, Z.; Weber, J. The Effect of the Double Layer on the Rate of the Fe^{3+}/Fe^{2+} Reaction on a Platinum Electrode and the Contemporary Electron Transfer Theory. *J. Electroanal. Chem.* **1977**, *77*, 163−180.
(32) Weber, J.; Samec, Z.; Mareček, V. The Effect of Anion Adsorption on the Kinetics of the Fe^{3+}/Fe^{2+} Reaction on Pt and Au Electrodes in $HClO_4$. *J. Electroanal. Chem.* **1978**, *89*, 271−288.
(33) Iwai, M.; Majima, H.; Awakura, Y. Oxidation of Fe(II) in Sulfuric Acid Solutions with Dissolved Molecular Oxygen. *Metall. Mater. Trans. B* **1982**, *13*, 311−318.
(34) Gil, A. F.; Salgado, L.; Galicia, L.; González, I. Predominance-Zone Diagrams of Fe(III) and Fe(II) Sulfate Complexes in Acidic Media. Voltammetric and Spectrophotometric Studies. *Talanta* **1995**, *42*, 407−414.
(35) Gil, A. F.; Galicia, L.; González, I. Diffusion Coefficients and Electrode Kinetic Parameters of Different Fe(III) - Sulfate Complexes. *J. Electroanal. Chem.* **1996**, *417*, 129−134.
(36) Hitchcock, A. P.; Wen, A. T.; Rühl, E. Transition Metal 2p Excitation of Organometallic Compounds Studied by Electron Energy Loss Spectroscopy. *Chem. Phys.* **1990**, *147*, 51−63.
(37) George, S. J.; Van Elp, J.; Chen, J.; Ma, Y.; Chen, C. T.; Park, J.-B.; Adams, M. W. W.; Searle, B. G.; De Groot, F. M. F.; Fuggle, J. C.; Cramer, S. P. L-Edge X-ray Absorption Spectroscopy of Pyrococcus furiosus Rubredoxin. *J. Am. Chem. Soc.* **1992**, *114*, 4426−4427.
(38) Van der Laan, G.; Kirkman, I. W. The 2p Absorption Spectra of 3d Transition Metal Compounds in Tetrahedral and Octahedral Symmetry. *J. Phys., Condens. Matter* **1992**, *4*, 4189−4204.
(39) Wen, A. T.; Rühl, E.; Hitchcock, A. P. Inner-Shell Excitation of Organoiron Compounds by Electron Impact. *Organometallics* **1992**, *11*, 2559−2569.
(40) Cressey, G.; Henderson, C. M. B.; Van der Laan, G. Use of L-edge X-ray Absorption Spectroscopy to Characterize Multiple Valence States of 3d Transition Metals; a New Probe for Mineralogical and Geochemical Research. *Phys. Chem. Miner.* **1993**, *20*, 111−119.
(41) De Groot, F. M. F. X-ray Absorption and Dichroism of Transition Metals and Their Compounds. *J. Electron Spectrosc. Relat. Phenom.* **1994**, *67*, 529−622.
(42) Huse, N.; Kim, T. K.; Jamula, L.; McCusker, J. K.; De Groot, F. M. F.; Schoenlein, R. W. Photo-Induced Spin-State Conversion in Solvated Transition Metal Complexes Probed via Time-Resolved Soft X-ray Spectroscopy. *J. Am. Chem. Soc.* **2010**, *132*, 6809−6816.
(43) Lange, K. M.; Kothe, A.; Aziz, E. F. Chemistry in Solution: Recent Techniques and Applications Using Soft X-ray Spectroscopy. *Phys. Chem. Chem. Phys.* **2012**, *14*, 5331−5338.
(44) Hatsui, T.; Shigemasa, E.; Kosugi, N. Design of a Transmission Grating Spectrometer and an Undulator Beamline for Soft X-ray Emission Studies. *AIP Conf. Proc.* **2004**, *705*, 921−924.
(45) Coreno, M.; de Simone, M.; Prince, K. C.; Richter, R.; Vondráček, M.; Avaldi, L.; Camilloni, R. Vibrationally Resolved Oxygen K → Π* Spectra of O_2 and CO. *Chem. Phys. Lett.* **1999**, *306*, 269−274.